Results obtained with the first four gap MWPC prototype chamber

David Hutchcroft, Anatoli Kashchuk[1], Werner Riegler, Burkhard Schmidt, Thomas Schneider, Vsevolod Suvorov[1]

European Laboratory for Particle Physics (CERN), CH1211 Genève 23, Switzerland

[1]On leave from PNPI, Gatchina Russia

Bernard Maréchal, Miriam Gandelman

Instituto de Física, Universidade federal do Rio de Janeiro, Rio de Janeiro, Brazil

Abstract

Results of measurements made with a full size four gap multi-wire proportional chamber prototype for the inner part of the LHCb muon system are presented. Comparisons between the calculated and measured detector capacitances of the wire and cathode pads have been performed. The efficiency and cross talk in the case of a combined anode-cathode readout of the prototype were measured in a test beam. In general the properties of the chamber are well understood, although the causes of instability of the system at low thresholds needs to be resolved. The prototype fulfils the requirements for the LHCb muon system. These results include data up to April 2001 updating a previous note.

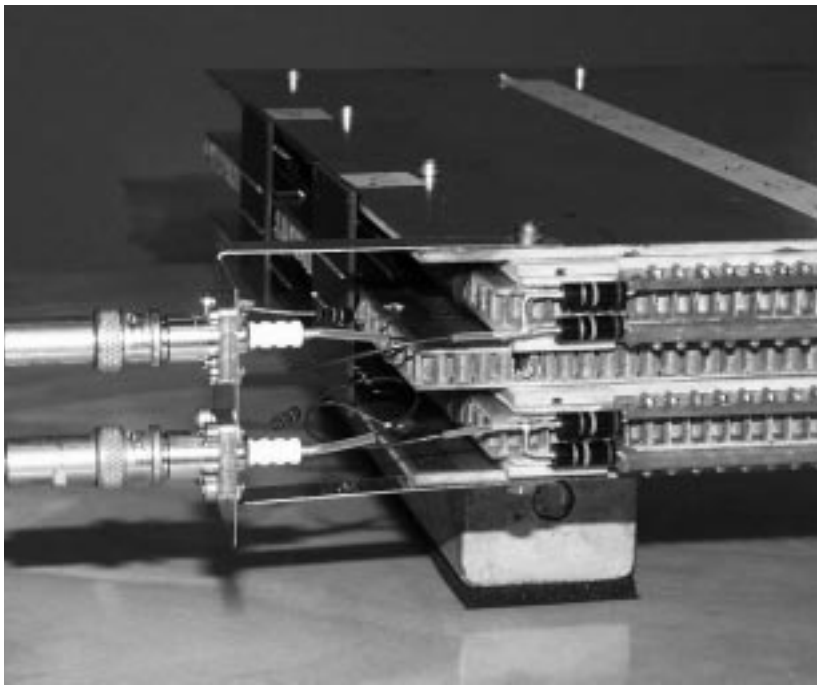

A picture of the chamber by the end of the assembly period.

1 Introduction

A large part of the LHCb Muon System will be equipped with Multi-Wire Proportional Chambers (MWPCs). The detectors in region 4 will have anode wire readout, those in region 3 and the inner part of stations 4 and 5 cathode-pad readout, while those in the inner part of stations 2 and 3 have a combined anode-cathode readout [1]. While in the first two cases the anode or cathode signals alone provide the space point, in case of the combined readout the anode signals are used to measure the horizontal coordinate and the cathode signals provide the vertical coordinate. The need for a combined readout is a consequence of the high granularity required in the horizontal plane (6 mm in station 2 region 1) and a less stringent requirement on the vertical plane (31 mm station 2 region 1). The high granularity leads to a high density of readout channels in these regions. Moreover, the combined readout makes these chambers particularly subject to cross talk [2]. Therefore, the electrical properties of these chambers and the Front End (FE)-interface have to be well understood.

Based on these considerations, a MWPC prototype was constructed as an example of the detector planned for use in region 2 of Muon station 2, with part of the wire-strip granularity matching the requirements for region 1 (see section 2 for a more complete description). The prototype has four separate sensitive gaps, each with an anode wire plane and a plane of cathode pads. The chamber readout was arranged such that the signals on both the anode wires and cathode pads could be measured simultaneously. The chamber had some cathode pads grounded and also the possibility to connect the wires to ground. This allowed the measurement of the chamber response with only the anode or cathode active, and hence a comparison with the results obtained from the combined readout.

The gaps were electrically connected in pairs before the readout chip giving two independent double gaps. Two FE-boards were available each allowing 16 channels to be read out. The interface to the chamber was arranged so that the 8 channels in one double gap and the corresponding 8 in the other were monitored.

The total and mutual capacitances of the anode and cathode channels were measured and compared to results obtained with the MAXWELL simulation, as discussed in Ref. [2] (see section 2.4). The measurements of the capacitances, which were done after the beam tests, revealed also some faults in the chamber which occurred during the chamber construction and helped to understand some of the obtained results.

Measurements of the chamber performance in the T11 and T7 testbeams at the CERN PS were made in November 2000 and April 2001. The chamber was tested to ascertain the double gap and quad gap efficiencies for anode wire “pads”, cathode pads and with the combined readout, see section 3.3. Also the effects of cross talk and noise are investigated, see section 3.4.

2 Detector description

2.1 General layout

A schematic view of the prototype is given in figure 1. The sensitive area of the chamber is $600 \times 250\,\mathrm{mm}^2$, corresponding to the chamber size in station 2 region 2. The prototype has 4 separate gaps, each with an anode wire plane and a plane of cathode pads. The values for basic chamber parameters are the following:

- 5 mm symmetric gas gaps
- Wire spacing 1.5 mm
- Gold-plated tungsten wires of 30 μm diameter from LUMA

Detailed simulation studies, summarised in [3, 4] show that the required detector performance can be obtained with these parameters.

Figure 2 shows two cross-sections of the chamber. The inner panel sandwiches are built of two printed circuit boards (PCBs) glued on a honeycomb sheet. The top and bottom panels are 3.2 mm thick FR4 sheets with copper cladding. The FR4 sheets were used in an attempt to simplify the construction, however they are less flat than the honeycomb panels. Also shown in the left figure are a gas inlet and outlet and in both figures the interface to the FE-electronics boards.

In the right hand diagram of figure 2 one can see a cross section of the chamber along the wire length. The gas volume of the chamber is closed with O-rings to ease re-opening of the chambers and allow for possible modifications.

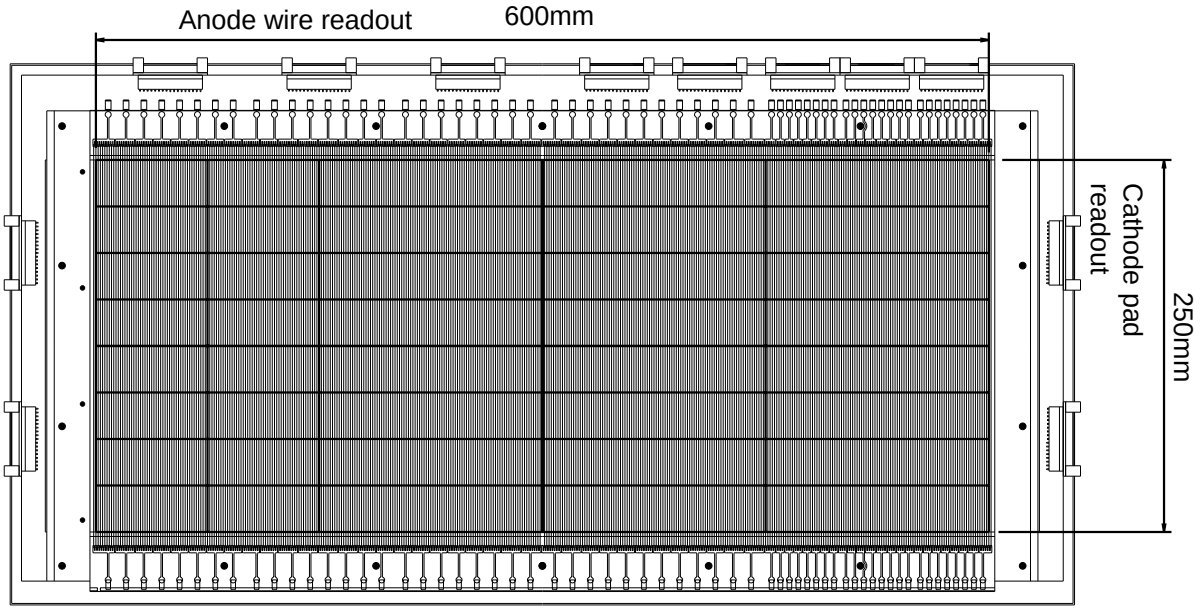

Figure 1: Top view of the wire plane laying over the cathode plane.

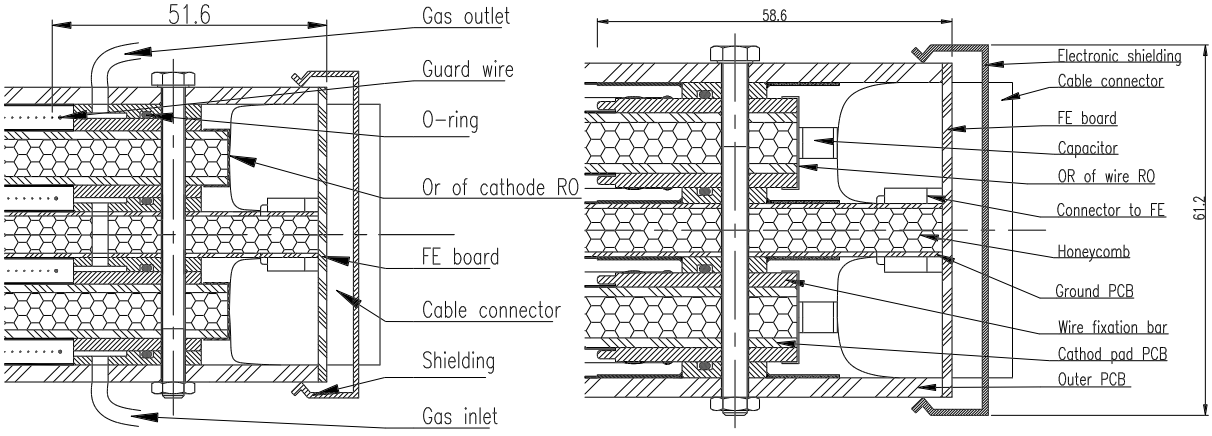

Figure 2: Two detector cross sections perpendicular (left) and parallel (right) to the wire planes. Shown in detail are the cathode pad readouts and the anode wire readouts in the left and right figures respectivly.

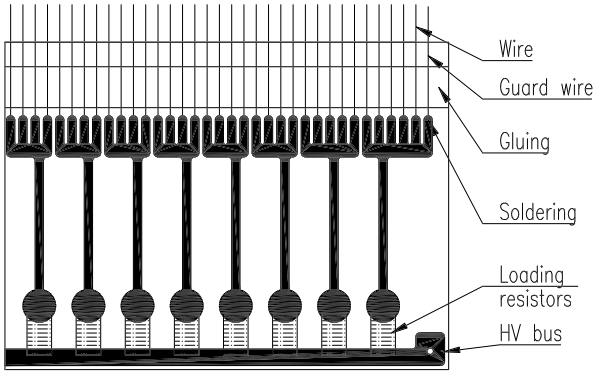

Figure 3: Blow up of a corner of the wire fixation bar.

The high voltage is brought to the wire pads via a bus line and individual loading resistors along the wire fixation bar, as can be seen in figure 3. The figure also shows how the wires are glued and soldered to the wire fixation bars.

The dimensions for the various components of the prototype are summarised in table 1.

2.2 Signal readout

As mentioned before, the prototype was built to study the combined anode-wire and cathode-pad readout. In both cases two neighbouring gaps were OR-ed before the signals were fed into the FE-boards. The anode wire signals are readout along the wires on the long side of the chamber, while the cathode pad signals are readout perpendicular to the wire direction on the short side of the chamber (see figure 1).

2.2.1 Anode wire readout

The chamber has two different wire strip sizes: $6.25 \times 250\,\mathrm{mm}^2$ and $12.5 \times 250\,\mathrm{mm}^2$. Figure 3 shows a corner of one of the wire planes and illustrates the grouping of wires in the small wire pads on the wire fixation bars. In order to obtain the required granularity with a uniform wire spacing of 1.5 mm, 4 or 5 wires are grouped together for the narrower wire strips with an average width of 6.25 mm. In case of the larger wire strips with an average width of 12.5 mm, 8 or 9 wires are grouped together.

2.2.2 Cathode pad readout

Figure 4 shows a drawing of the cathode pad plane where the cathode pads are numbered according to the readout sequence. The larger cathode pad dimensions are $150 \times 31.25\,\mathrm{mm}^2$ and the smaller pad dimensions are $75 \times 31.25\,\mathrm{mm}^2$. The readout traces and a column of the larger pads that were grounded are also shown in figure 4. All the other lines shown in the drawing are guard ground lines introduced to minimise the mutual capacitances and hence cross talk effects [2]. This is discussed further in section 2.4.

2.3 Construction procedure

The construction was done following the steps summarised below.

- **Panels:** The flatness of the printed circuit boards (PCB) and the honeycomb sheets was controlled before the panel gluing. Only the components with a flatness within $\pm 50\mu$m were accepted. About 20% of the PCBs were outside this specification. The chosen PCBs were glued to the honeycomb sheets with Araldite 2011, and then left for about 24 hours held to a flat surface by vacuum. The flatness of the final panels was measured again. The measurements showed a maximal deviation of $\pm 50\mu$m with an RMS of the measurement of about 20μm. These measurements are within the required tolerances.

- **Frames:** In order to avoid surface currents the wire fixation bars were first machined with a special profile in order to smooth the electric field at the borders. They were then glued on the panels with the cathode structure, while the bars with the O-ring grooves were glued on the central panel and the two outer FR4 sheets.

- **Wiring:** First a 100μm guard wire was placed by hand at each end of the chamber and their wire tension was adjusted to 300 g. The guard wires were positioned to have a 1.5 mm offset from the sense wires. The wiring of the plane was done in a standard winding machine. In a first step a frame with precise combs (to insure the correct wire spacing) was mounted to the machine and

Outer chamber dimensions	$715 \times 362 \times 62\,\mathrm{mm}^3$	Sensitive area	$600 \times 250\,\mathrm{mm}^2$
Number of gaps	4	Gap size	5 mm
Number of Anode channels	2×32	Number of Cathode channels	2×60
Number of wires	4×400	Wire pitch	1.5 mm
Honeycomb thickness	7 mm	Outer PCB thickness	3.2 mm
Cathode PCB thickness	1.6 mm	Ground PCB thickness	0.8 mm
Wire pad sizes	$6.25 \times 250\,\mathrm{mm}^2$	Cathode pad sizes	$75 \times 31.25\,\mathrm{mm}^2$
	$12.5 \times 250\,\mathrm{mm}^2$		$150 \times 31.25\,\mathrm{mm}^2$

Table 1: MWPC prototype parameters.

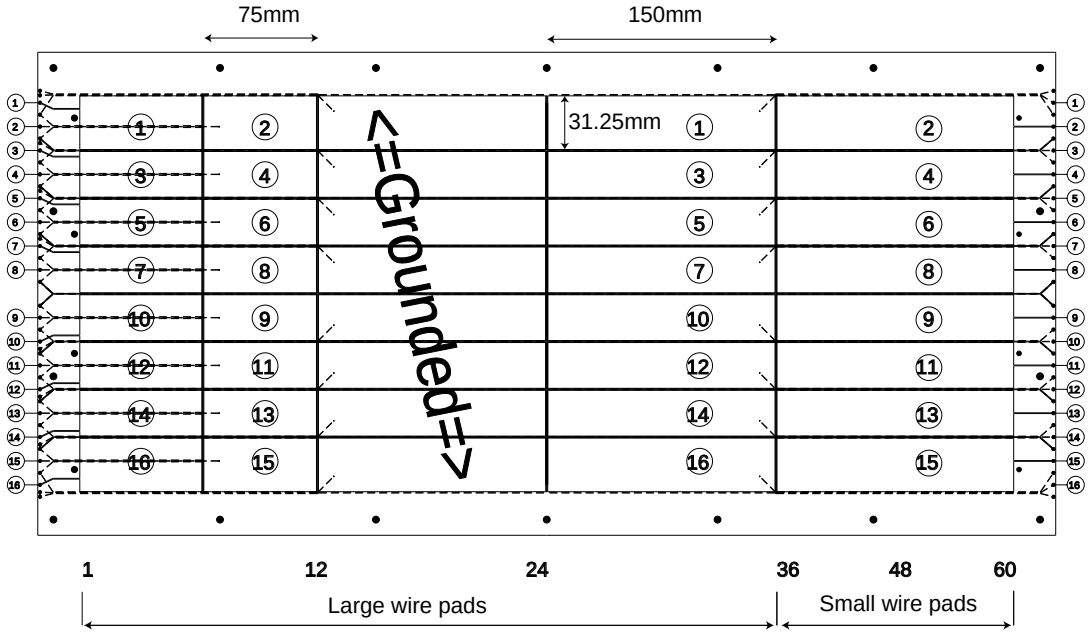

Figure 4: Top view of the cathode plane. The circled numbers indicate the connection between readout traces and cathode pads. This numbering scheme is used for the chamber capacitance measurements.

wired. The wire tension was 50 g. Next the two wire planes produced were transfered to intermediate frames. Finally, these planes were put on top of the honeycomb sandwich. To guarantee a distance of 2.5 mm from the wire plane to the cathode, the height of the frame carrying the wires was adjusted using a microscope. The wires were then glued with Adekit 145A and left for 24 hours allowing the glue to polymerise.

- **Soldering:** The wire soldering was done manually with a low temperature solder. An additional flux paste was used to allow a faster and easier soldering. The same paste was used to solder the front-end components and this caused serious problems. The conductivity of the paste was higher than expected and all the connectors and capacitors had to be replaced. A different solder was then used.

- **Assembling:** Before the final assembling of the chamber, all the panels were cleaned with an ionising nitrogen gun. The closing of the chamber with screws caused slight deformations on the corners of the sandwich panels. For future prototypes a reinforcements of these border regions is foreseen.

The gas system was not capable of ensuring reliable gas flow through all four gaps. In the measurements made during the testbeam it became clear that one double gap (labelled A) was systematically worse than the other double gap. This was traced in the April testbeam to a single gap on the outside of the chamber. One possible explanation is that the outer panel is not sufficiently flat and has changed the gas gap width.

2.4 Detector capacitances

The pad-ground capacitances and pad-pad capacitances where measured using a voltage sine wave generator. For the capacitance measurement of a single pad, all the other electrodes in the chamber were grounded. Unfortunately these measurements were only done after the testbeam data taking in November, so problems like unconnected or shorted pads that where discovered during the capacitance measurements are present in that data. The chamber was repaired before the April testbeam measurements. The overall chamber geometry is shown in figure 4. Figure 5 shows the wire pad capacitances. The 1.25 cm wire pads have a capacitance of $\sim$40 pF, the small pads show $\sim$25 pF. The 20% discrepancy with the calculation is most probably due to edge effects. All the capacitances outside the nominal values where identified with mechanical errors, i.e. unconnected or shorted pads.

The mutual pad-pad capacitances are shown in figure 5. The capacitance is $\sim$2.5 pF, independent of the pad size as expected. The value is 40% higher than the calculated one. It is however still not in a critical range.

The capacitances of the small cathode pads to ground are shown in figure 6. The capacitance of $\sim$58 pF is 20% larger than the calculated value. The mutual pad-pad capacitance is shown in figure 6. The measured numbers agree very well with the calculation. The measured value was 1 pF between pads 1-3, 2-4, 3-6 etc. and 3.6 pF between pads 1-2, 3-4 etc., see figure 4. The large capacitance between pads $1-2$ etc. is due to the readout trace of pad 2 that runs under pad 1. The fact that this number agrees well with the calculation is a very important result since the readout for all the chambers is region 1 and region 2 is based on this scheme.

Finally figure 7 shows the capacitances of the large cathode pads to ground which are alternating due to the different readout trace configurations. The numbers agree well with the calculation. All the numbers outside the nominal values were identified with mechanical faults.

We conclude that except for the wire pad mutual capacitances all measured values agree with the calculations within 20%. The high mutual wire pad capacitances of 2.5 pF are still well within allowable tolerances.

2.5 Front end electronics

The front end (FE) electronics are based upon the ASDQ++ readout scheme as described in Ref. [5]. The addition of a common base transistor in front of the each input to the ASDQ chip reduces the input impedance and extends the valid range of detector capacitances. The noise characteristics were also reduced by this modification. A schematic of

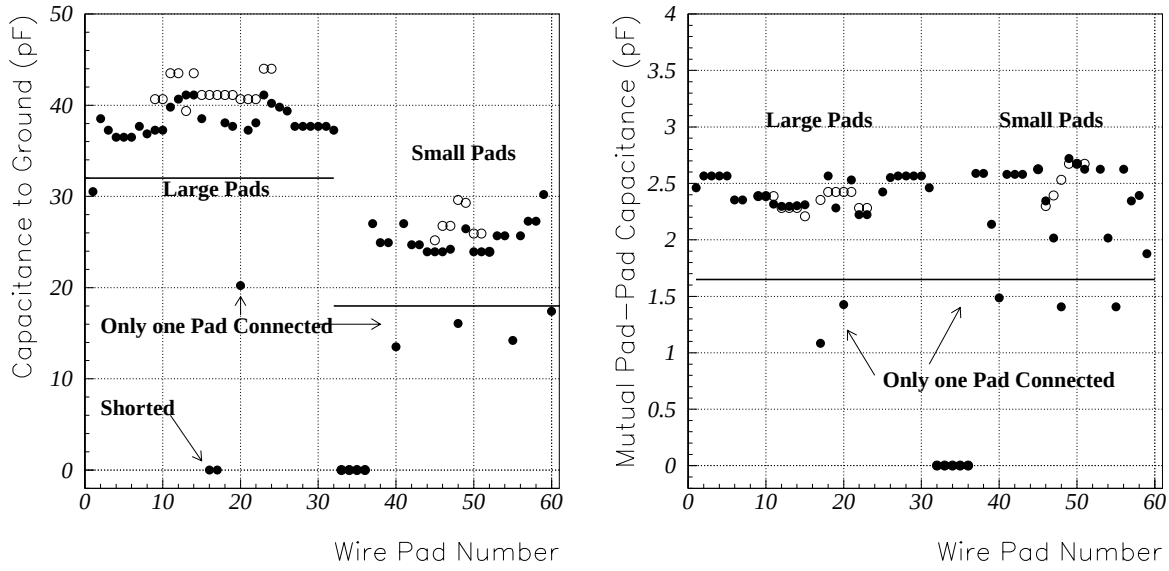

Figure 5: The left plot shows the wire-pad capacitances to ground. On one double gap, not all the pads were measured. The numbering scheme follows figure 4. The pads showing a capacitance of zero are grounded. The right plot shows the mutual wire-pad to wire-pad capacitance. As expected the capacitance is independent of the wire pad size. The values smaller than 2.5 pF were identified with mechanical faults. The solid line shows the calculated value which is 40% lower than the measured one. The solid lines show the calculated values and the solid and open circles refer to the measurements of the two different double gaps.

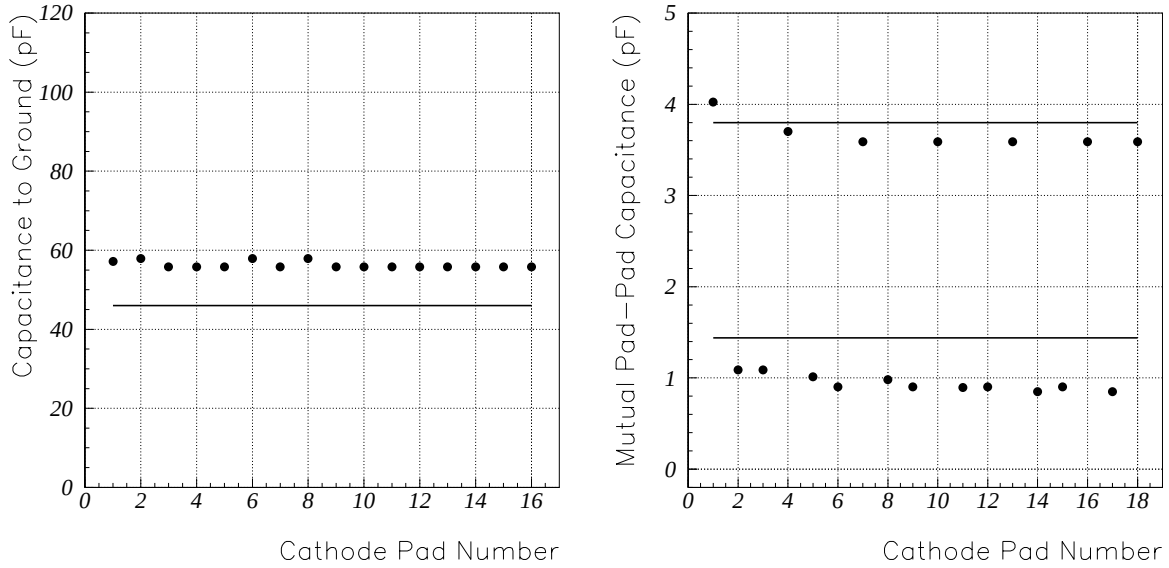

Figure 6: The left plot shows the capacitances of the small cathode pads to ground. The measured numbers (points) are $\sim 20\%$ larger than the calculated ones (line). The larger capacitance between pads is due to the readout traces running under the neighbour pad. Only one double gap was measured.

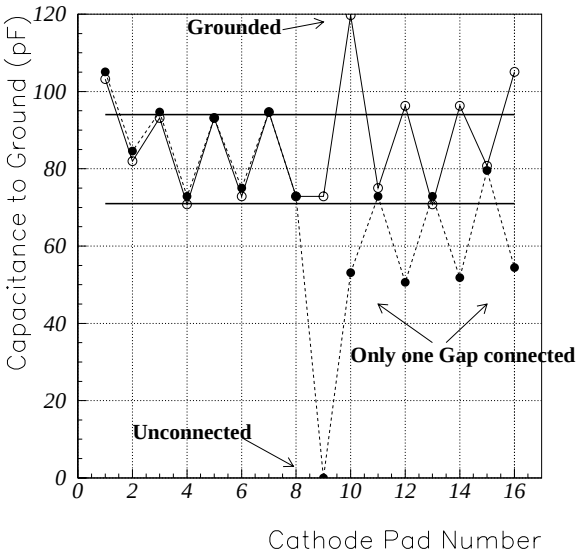

Figure 7: Capacitance of the large cathode pads. The measurements (points) agree well with the calculations (lines). Small edge effects are clearly visible. The values different from the nominal ones were identified with mechanical problems. The solid and open circles refer to different double gaps.

the design of the readout for the anode wires and the cathode pads is shown in figure 8. This shows the hardwired OR of each double gap before the amplifier and the conversion to LVDS to send the signals to the DAQ system. Only the digital ouput of the electronics were recorded.

The FE electronics have been implemented in two stages; the first stage as a spark protection board (SPB) and the second as the ASDQ chip board (ACB). The ACB is mounted parallel to and immediately above the SPB. This design limits the distance the signals must propagate from the chamber. Only the digital outputs of the chambers were recorded. The ACB design has undergone several improvements since the testbeam data was taken.

Another technical note will describe the FE electronics in detail with a full schematic [6]. This will contain the details of the implementation and the response of the FE electronics. Here only those measurements related to the chamber response in the testbeam are mentioned.

2.5.1 Spark protection board

The SPB is a $50\times60\,\mathrm{mm}^2$ 2 layer 16-channel board that contains a system of resistors and diodes for each channel designed to limit the voltage in the event of a spark or discharge. The design uses a two stage double diode scheme: the first resistor is $8.2\,\Omega$[1] connected to two diodes[2] and a second resistor of $5\,\Omega$[3] was also connected to two diodes[2]. This design fully protected the readout channels during measurements up to 3.6 kV on the chamber and from discharges of a 1000 pF capacitor. During the testing no channel became damaged in contrast to the simpler scheme described in Ref. [5]. The noise suppression resistor and capacitor for each channel are $15.2\,\Omega$ and 17 pF respectively.

2.5.2 ASDQ chip board

The ACB is a $50\times60\,\mathrm{mm}^2$ 4 layer 16-channel PCB containing 16 common base transistors[4] and two ASDQ chips. The noise characteristics of the readout are improved with respect to the previous implementation [5]. The parallel noise was reduced by increasing the resistance of the collector and

[1] SMD 2512, 1 W
[2] BAV99
[3] SMD 1206, 0.25 W
[4] BFR-93A

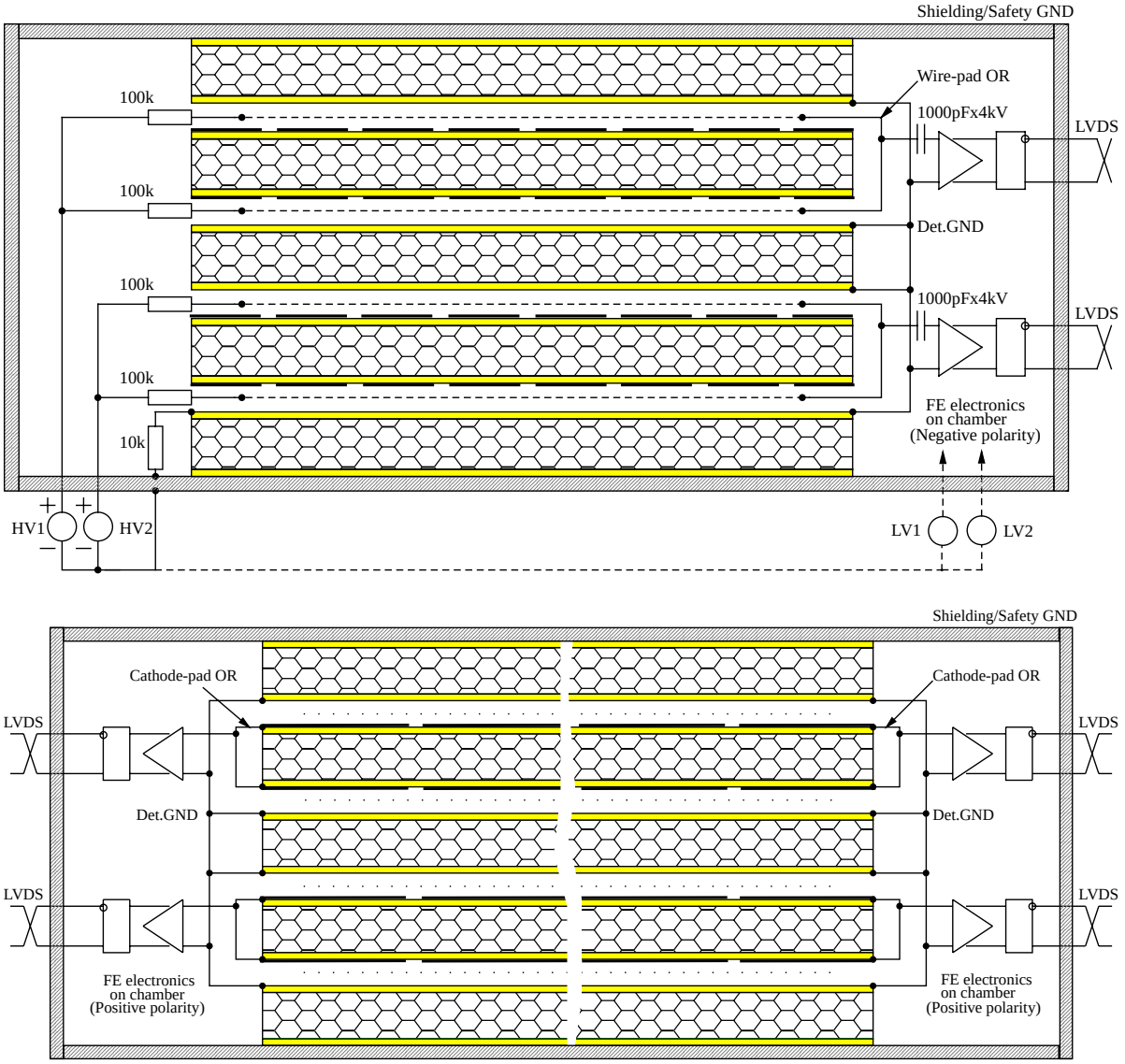

Figure 8: A schematic view of the wire pad readout chain in the upper diagram and the cathode pad readout chain in the lower diagram. The HV is shown on the wire pad readout. The upper plot shows a vertical section though the chamber with the wires running parallel to the page, the lower plot shows a horizontal section with the wires perpendicular to the page.

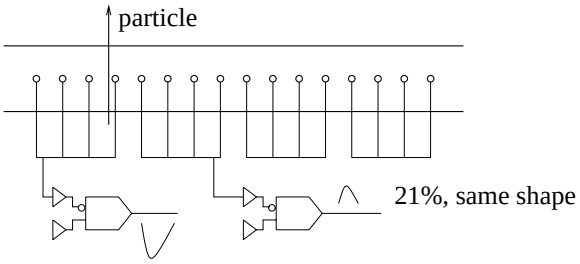

Figure 9: The electrons inducing a negative signal on one wire induce a positive signal on the neighbouring wire which causes problems at the edge of the wire pads.

emitter resistors supplying the first transistor. The series noise was reduced by reducing the total resistance in the SPB.

2.6 Baseline restorer response

Each channel of the ASDQ chip has two preamplifiers connected to a differential amplifier. Depending on the polarity of the input signal one connects one of the two in order to have the same polarity for the chip-internal signal processing chain. One problem arising for the wire pads is shown in Figure 9. If a particle crosses the edge of a wire pad, all the electrons will drift to the edge wire and induce a negative signal there. The charge of the avalanche however also induces a positive signal on the edge wire of the neighbouring pad which has the same pulse shape, opposite polarity and 21% pulse height of the negative signal. The result is a positive input signal into the 'negative' amplifier input which causes a positive signal in the internal signal processing chain. The response to this 'wrong polarity' signal of the chip is shown in figure 10 for two settings of the BLR response range. In a balanced mode the response to different polarities is equal. If the response is optimised for a given input polarity (negative in figure 10) and the opposite signal is provided there is an initial small pulse in that direction followed by a large and long response in the opposite sense. This can cause signals delayed by about 75 ns from the initial pulses, compared to about 59 ns for signals of the correct polarity. In the November testbeam data was taken with the BLR optimised for the expected polarity, in the April testbeam the data was taken with a balanced system.

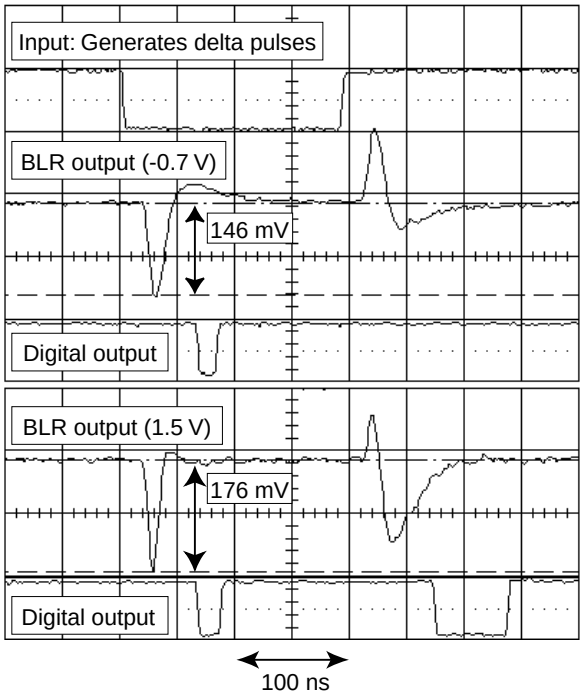

Figure 10: The figure shows the output of the baseline restorer (BLR) and discriminator for the negative ASDQ++ board. The upper trace indicates the inputs to a circuit to generate equal and opposite delta pulses. With the BLR response balanced with an input control voltage of -0.7 V the analogue and digital outputs are shown in the 2nd and 3rd trace. If the BLR is set to maximise the response for negative signals, control input of +1.5 V, the responses are shown in the two lowest traces. Each horizontal division is 50 ns.

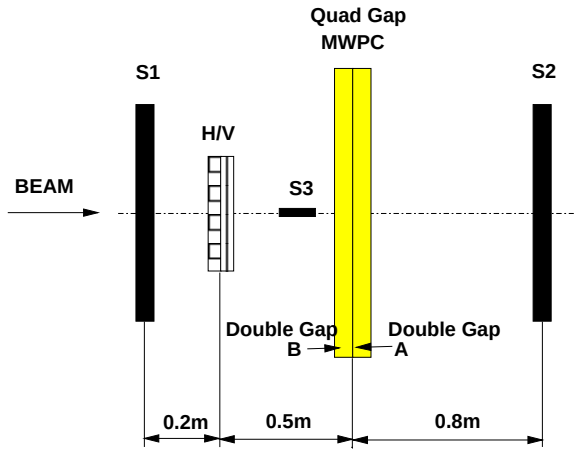

Figure 11: The layout of the 3 scintillators, the hodoscope and the chamber in the testbeam areas. The trigger was set for a coincidence between the scintillators S1, S2 and optionally a specific horizontal and vertical hodoscope strip. The small scintillator S3 was used in T11 in November but not subsequently.

3 Testbeam results

3.1 Experimental set-up

Data was taken in the T11 test beam from October 31st 2000 until November 7th and from the 24th to the 29th of November in T7. Additional data with the modified electronics and repaired chamber were taken from April 6th to 9th 2001. The experimental set up is shown in figure 11. A detailed description of the DAQ can be found elsewhere [5]. The default trigger was based on a coincidence of the scintillators S1 and S2, with an additional coincidence with the small scintillator S3 in the first period. In the second period a vertical and a horizontal channel of the hodoscope were used in coincidence with with the S1 and S2 scintillators in the data analysis. The trigger was delayed by 300 ns to allow both the history and the subsequent signals to be observed. TDCs measured the time of hits in the scintillators, the hodoscope and the chamber. Scalers counted for 333 ms of the 400 ms burst to record the total numbers of hits in the scintillators, the hodoscope and the chamber.

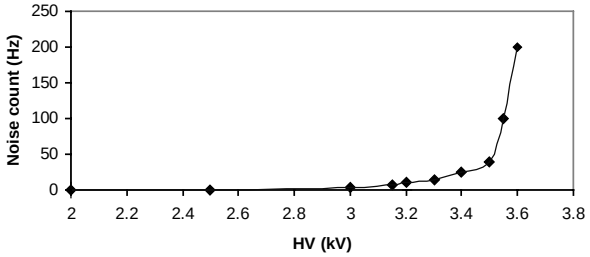

Figure 12: The noise rate for the chamber as a function of the HV, in the November configuration. These measurements were taken without beam.

3.2 Chamber hit multiplicities

Figure 12 shows the noise rate for the chamber without beam as a function of the applied HV. However very high signal rates were seen during data taking. This was predominantly due to instability in the system which induced large hit rates when the beam was on. The hit rate was directly proportional to the beam intensity for each HV setting and the spills without beam show almost no hits in the chamber.

The dE/dx feature of the ASDQ chip [5] was on in November; in this mode the length of the output pulse is proportional to the measured charge. The dE/dx feature also increases the dead time hence suppressing the hits immediately after a signal. At larger HV the longer average pulse length contributed to the larger dead time. In April owing to better stability in the system the dE/dx feature was off and the ASDQ provided short output pulses.

3.3 Efficiency results

The requirement for the quad gap MWPC is to provide signals with over 99% efficiency for a minimum ionising particle crossing the chamber. There is also the requirement of over 95% efficiency with only one double gap. The final readout will logically combine the two double gaps to increase the efficiency and provide redundancy. So both the single double gap and double double gap (hereafter double and quad gap) efficiencies were measured. The plateau length is the range of high voltage (HV) in which the double gap is at least 95% efficient and does not spark or draw significant dark current.

The chamber is designed with a gas gain of $1 \cdot 10^5$ as the nominal operating point. The chamber should be efficient if the gas gain were to vary between $(0.5 - 2) \cdot 10^5$ with the attendant changes in pulse size induced in the pads. The HV corresponding to these gas gains is 3.15 ± 0.15 kV. This indicates that the plateau ought to start at 3.0 kV for each of the readout configurations.

The efficiency for the two sizes of anode wire pad are shown in figure 13 as a function of the HV, these measurements were made opposite a grounded cathode plane. The trigger was based upon a 1 cm by 1 cm area in the hodoscope. The narrow size of the wire pads and the distance of the chamber from the hodoscope allowed triggered particles to spread into 3 wire pads. To accurately measure the efficiency the first hit in any of three adjacent wire pads was taken in November and four in April. The plots for the two sizes of cathode pads are also shown in figure 14, the measurements were also made with the anode wires grounded at HV. The same measurements with a combined readout are shown in figures 15 and 16.

The improvement seen between November and April is attributed to the significantly lower chamber noise. This indicated large dead times in November which reduced the overall efficiency. The measurements of the chamber in November show that there was no useful plateau for the cathode pads in combined readout mode and a limited plateau for the wire pads. Both were caused by an unstable readout that would sometimes "ring" for many repetitions after a particle induced a signal, this greatly increased the dead time. With the improved grounding in April these effects were no longer apparent.

At the nominal working point of 3.15 kV the efficiency was good ($>95\%$) for both of the double gaps in each readout configuration in April. The start of the plateau is about 2.95 kV for the wire pads. For the cathodes the plateau starts before 3.0 kV and there is no appreciable drop in efficiency up to 3.4 kV.

The effect of varying the time window in which signals are accepted was measured. Figure 17 shows the time distributions for the signal for both the large cathode pads ($3.1 \times 15\,\mathrm{cm}^2$) and the large wire pads ($1.25 \times 25\,\mathrm{cm}^2$) at both 3.15 kV and 3.40 kV. The efficiency as a function of the size of the acceptance window for these distributions and the dependence on the position in time of the nominal 20 ns window are also plotted. These plots show that the cathode pads at a low HV benefit from a larger time window, although in the plateau region both anode and cathode pads have saturated the efficiency in a 20 ns window. The ability to reposition the window with an accuracy of a few nanoseconds if the HV is changed can be seen to be important, particularly for the cathode pads.

3.4 Cross talk results

Cross talk between anode wire pad or cathode pads will reduce the positional sensitivity of the chamber. This has implications for the L0 muon trigger performance, the dead time and hence the efficiency. Therefore cross talk should be minimised at all stages in the detector design. In the following results from cross talk to one or more adjacent pads are presented.

In the testbeam data two types of cross talk were observed.

- **In-time cross talk :** A hit is found in an adjacent pad within the same time window.
- **Out-of-time cross talk :** An in-time hit is found in the pad crossed by the beam and another hit in an adjacent pad 20 ns later.

The explanation for the out-of-time cross talk was found in the response of the baseline restoration circuit to pulses of the opposite polarity to the ones expected by the pre-amplifier, as described in section 2.6.

The average cluster size for the anode wire pads and the cathode pads is show in figure 18, for data taken in April. This clearly shows that there was little cross talk in the anode wire pads and less in the cathode pads. However this was only achieved in the April testbeam after modifications to the chamber grounding scheme and electronics boards. The data taken in November shows much more cross talk and larger cluster sizes especially in the anode wire pads.

The cathode pads have capacitive couplings along each edge and between the readout traces and pads. Figure 4 shows that for the small cathode pads a scheme with the readout traces running under pads in the same horizontal row was tested. The small cross talk rate between cathode pads in

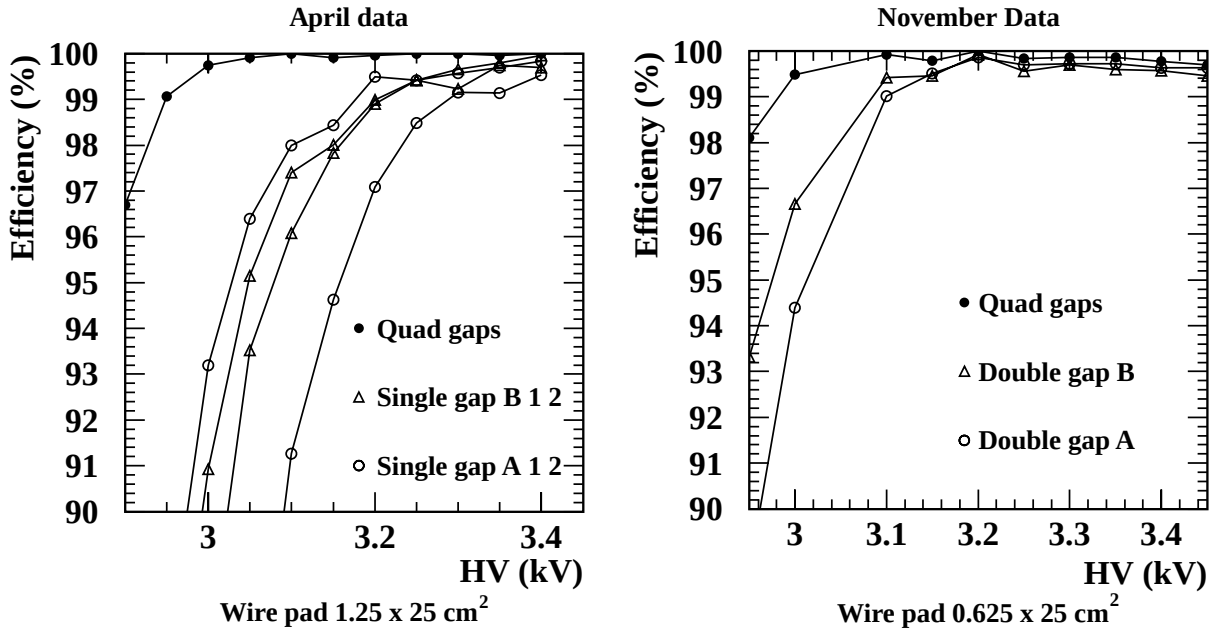

Figure 13: **Anode Efficiencies, Single Readout**: The efficiency is plotted for both sizes of wire pad. The threshold was set at 210 mV for the large wire pads and 270 mV for the small wire pads. The other side of the readout were grounded during these measurements.

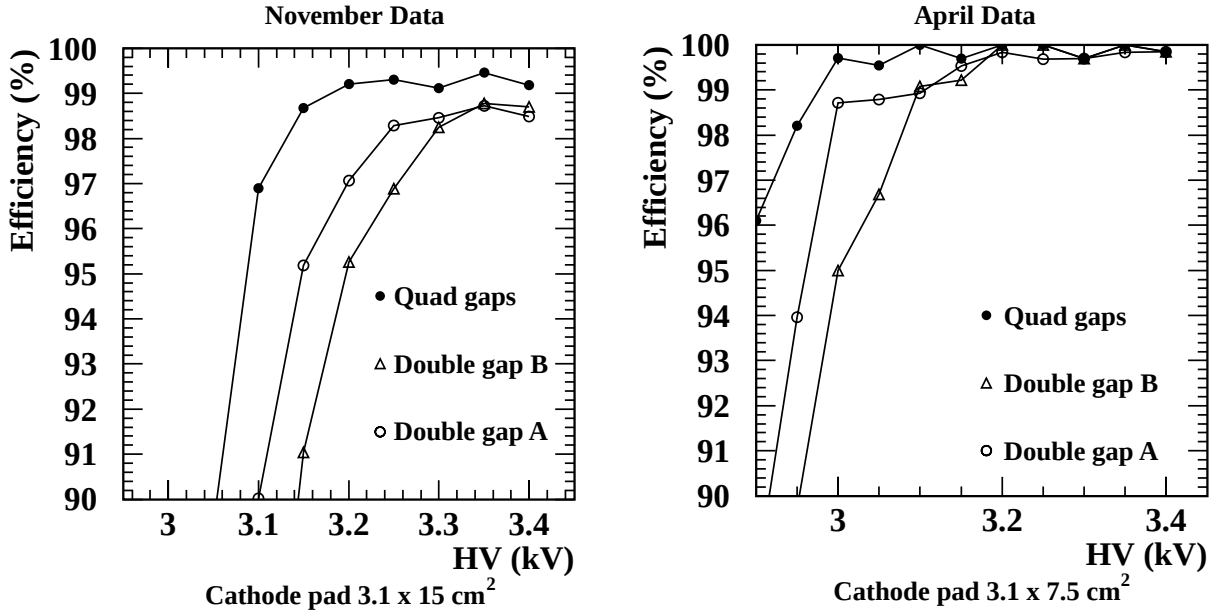

Figure 14: **Cathode Efficiencies, Single Readout**: The efficiency is plotted for both sizes of cathode pad. The threshold was set at 270 mV for the large cathode pads and 240 mV for the small cathode pads. The other side of the readout were grounded during these measurements.

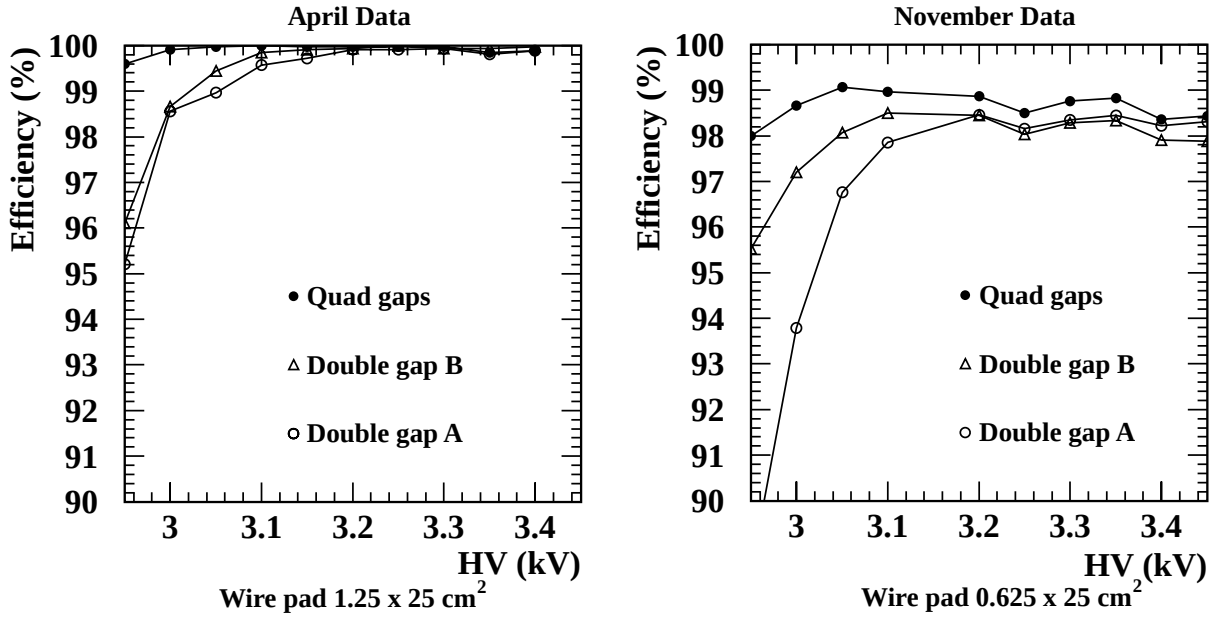

Figure 15: **Anode Efficiency, Combined Readout**: The efficiency for each of the two double gaps (A and B) and the combined quad gap is plotted for both sizes of wire pad. The threshold was 310 mV for the large pads and 250 mV for the small pads. In each case both anode and cathode planes were connected to the readout.

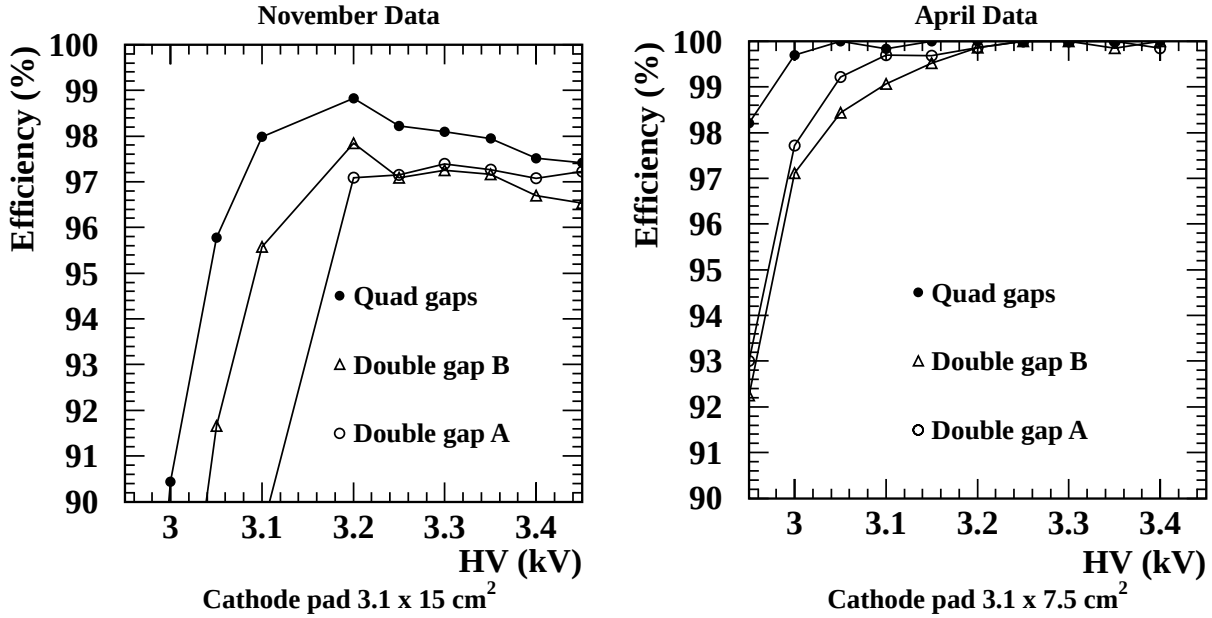

Figure 16: **Cathode Efficiency, Combined Readout**: The efficiency for each of the two double gaps (A and B) and the combined quad gap is plotted for both sizes of wire pad and cathode pad. The threshold was 250 mV for the both sizes of wire pads, 250 mV for the small cathode pads and 280 mV for the large cathode pads. In each case both anode and cathode planes were connected to the readout.

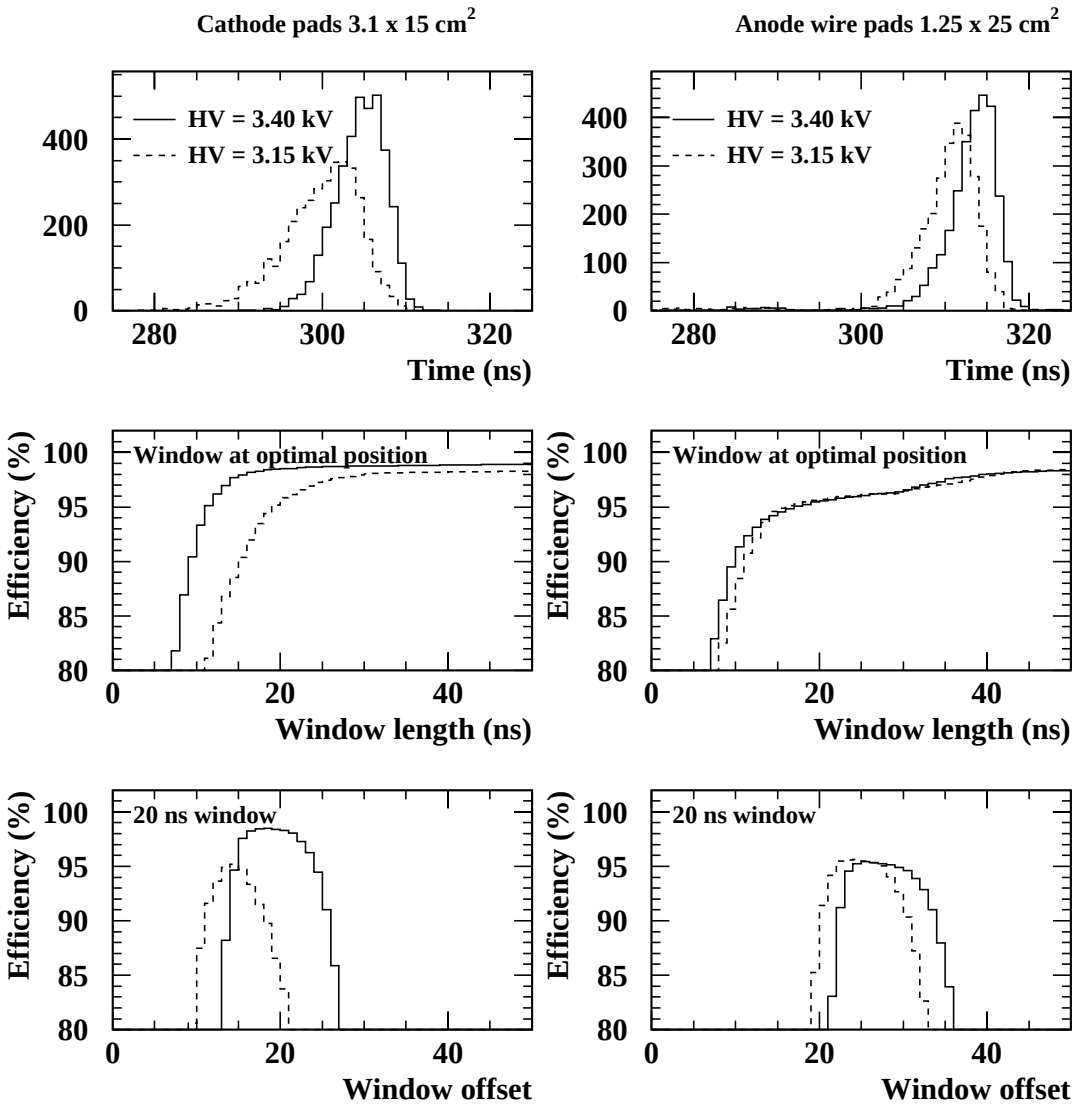

Figure 17: The top row of plots shows the time distributions for both $3.1 \times 15\,\mathrm{cm}^2$ cathode pads (left) and $1.25 \times 25\,\mathrm{cm}^2$ anode wire pads (right) at two HV settings. The efficiency for the chamber in this channel as a function of the acceptance window is shown in the centre row, only a single wire pad is sampled here so the lower efficiency can be understood as external triggers with the particle missing the wire pad. The position of the window was set at each point to maximise the efficiency. The lower row of plots shows the effect of scanning a fixed 20 ns window in time.

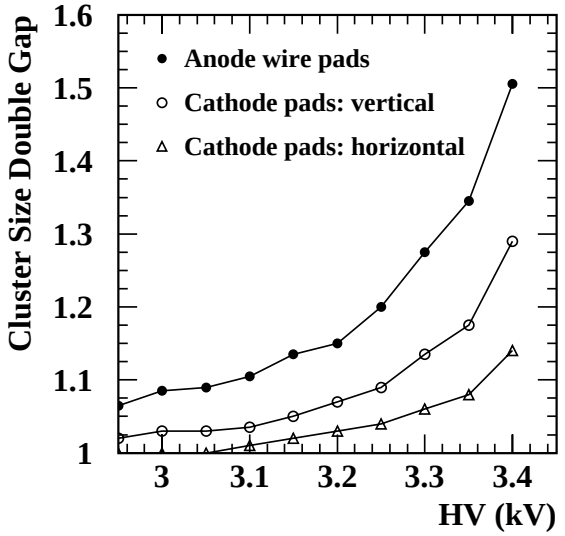

Figure 18: The average cluster size in the large anode wire pads and small cathode pads, data taken in April. The curves are the average of the two double gaps in combined readout mode. This data was taken after the improvements were made to the electronics.

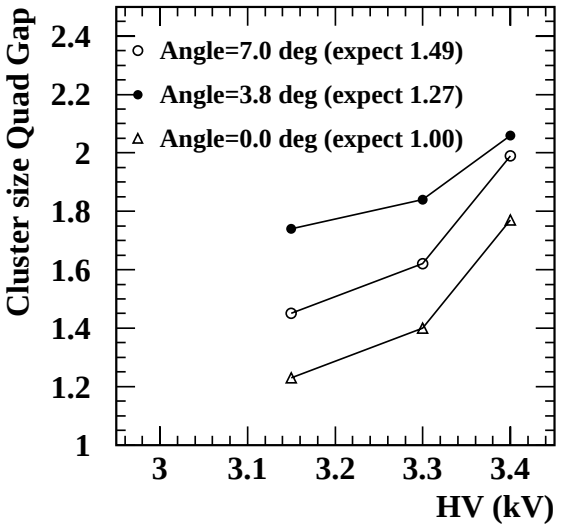

Figure 19: The average cluster size in the anode wire pads for three different particle incidence angles, data taken in April. The curves are the cluster size seen in the OR of the 2 double gaps. The numbers in brackets are the prediction from the purely geometrical cross talk.

the same horizontal row, as shown in figure 18, indicates that this configuration does not lead to significant cross talk.

The effect of geometrical cross talk was investigated, if the particles are not travelling perpendicular to the chamber they may pass from one channel in the front double gap to a neighbour in the back double gap. In the OR of the two double gaps this then gives a cluster size of greater than one. For a chamber with a distance of 50 mm between the start of the first sensitive gap and end of the last and a wire pad dimension of 12.5 mm the expected geometrical cluster size is $1 + 4 \tan\theta$ for a track of inclination angle θ. Figure 19 shows the size of the geometrical cross talk in the OR of the double gaps for three angles. The angle of the chamber was not measured in the November testbeam and so the effects of the geometrical cross talk can not be disentangled from the electrical cross talk. Only cross talk measurements with the chamber at 0° taken in April will be presented here.

The rates of cross talk are plotted in figure 20 and 21 in for combined readouts. Also shown in the same figure is the cross talk rates with an additional requirement of exactly one hit in the opposite double gap. This additional requirement resolves the problem of particles crossing pad boundaries, and tends to suppress correlated cross talk from ground oscillations for example.

The size of clusters was investigated, figure 22 shows the cluster sizes for the anode wire pads ($1.25 \times 25\,\mathrm{cm}^2$) with the normal trigger. This shows that the cross talk increases with the gas gain as the signal size become larger.

4 Conclusions

A multi wire proportional chamber prototype for the muon system was built and tested at CERN during the later half of 2000 and beginning of 2001. The chamber was a full size example of a chamber envisaged for parts of the muon system. The construction of the prototype proved the viability of the proposed scheme, however several areas for improvement were revealed which were partially address before the April testbeam. The development work is continuing and a new chamber suitable for M2R1 is in preparation.

The chamber design was simulated to under-

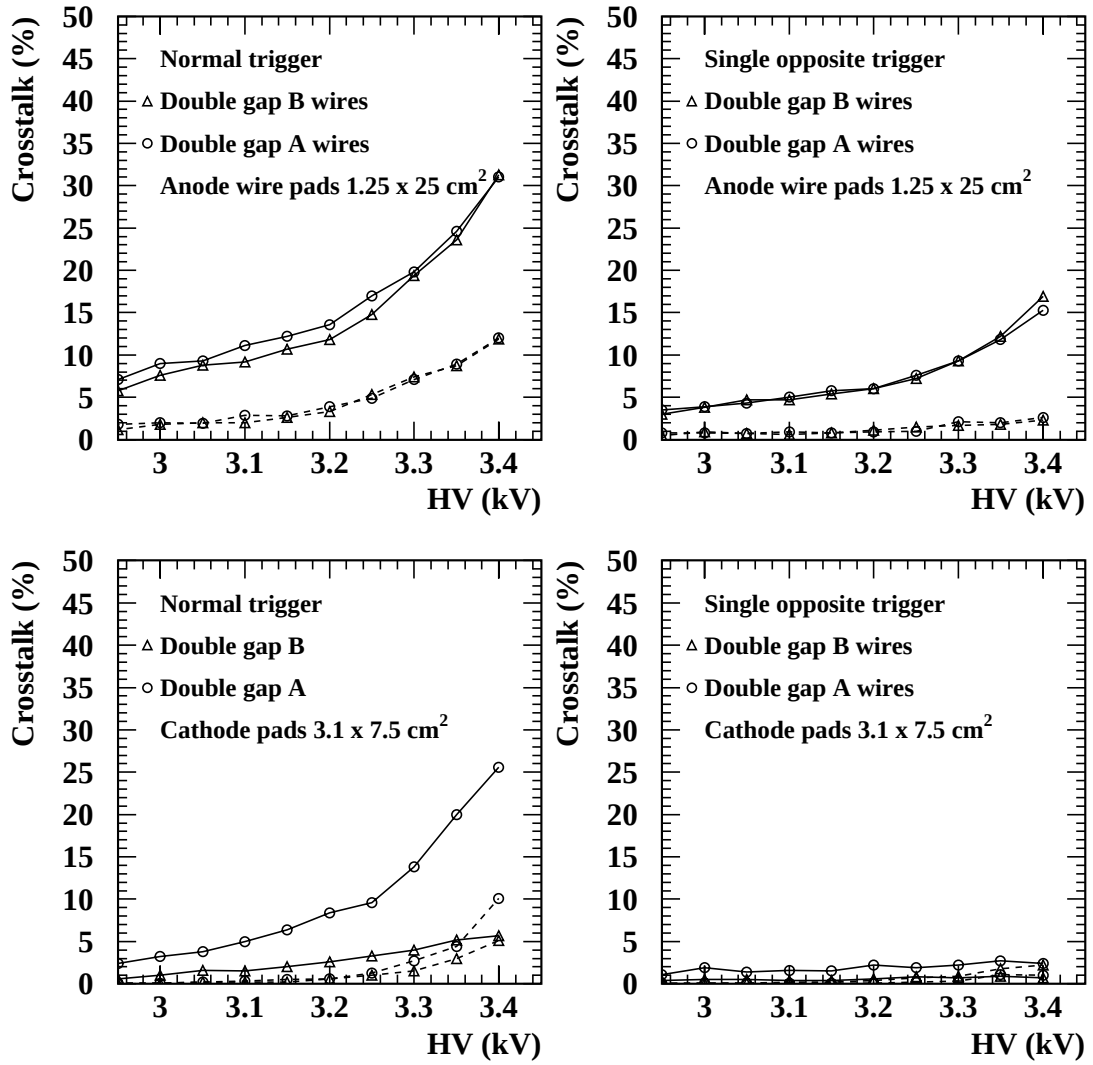

Figure 20: **In-time Cross talk**: The plots show the cross talk between each pad and its neighbour (solid curves) and next-neighbour (dashed curves), data taken in April. In the left column the normal trigger is applied, in the right a single pad cluster is required in the opposite double gap. This additional requirement reduces the geometrical cross talk and cases where many of the channels fire due to electrical instabilities in the readout electronics.

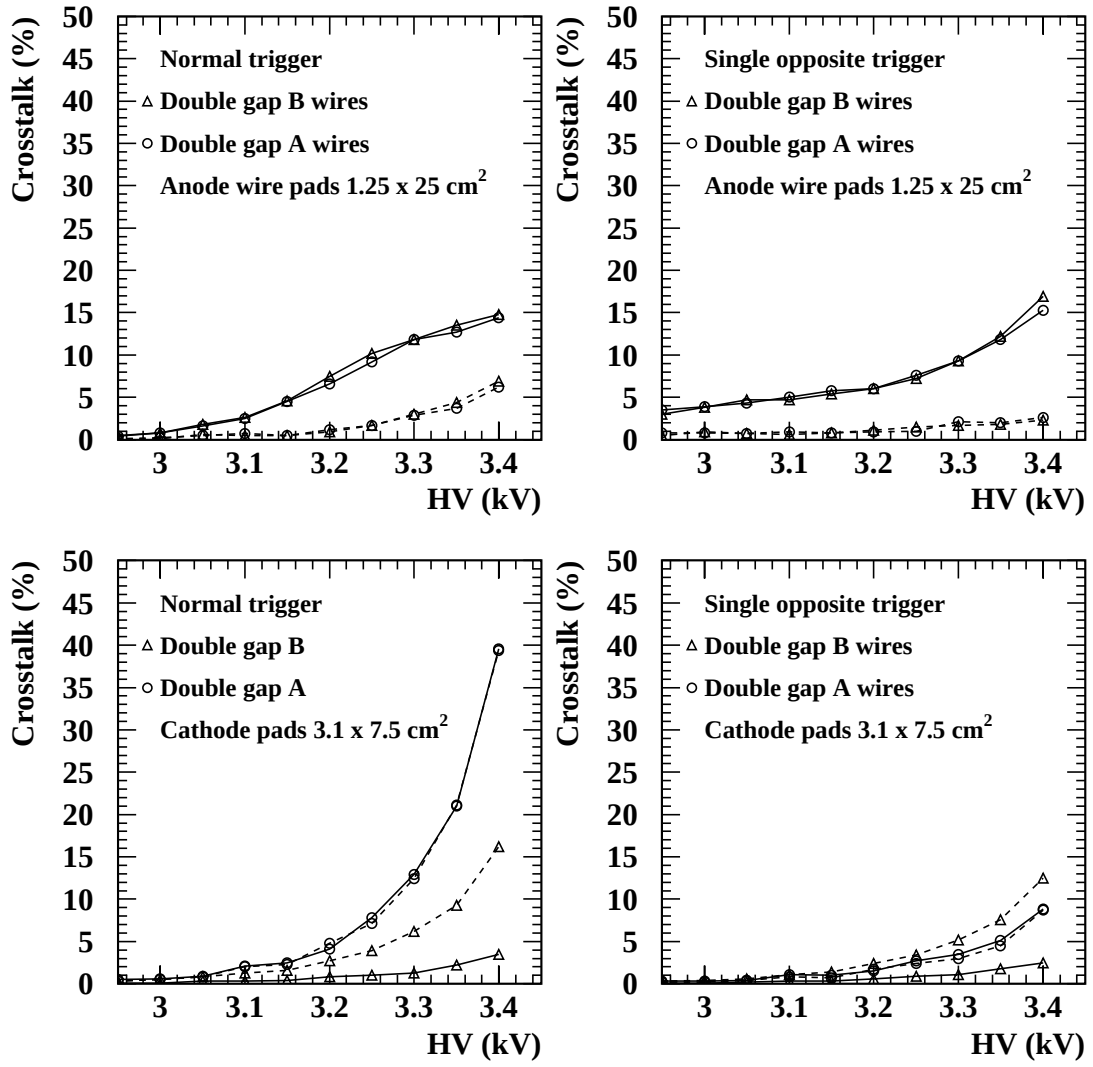

Figure 21: **Out-of-time Cross talk**: The plots show the cross talk between each pad and its neighbour (solid curves) and next-neighbour (dashed curves) in the next time bin (25–50 ns), data taken in April. In the left column the normal trigger is applied, in the right a single pad cluster is required in the opposite double gap. This additional requirement reduces the geometrical cross talk and cases where many of the channels fire due to electrical instabilities in the readout electronics.

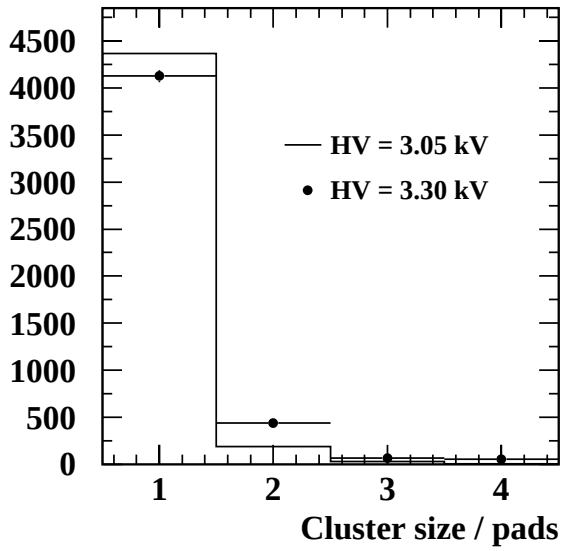

Figure 22: The size of the clusters crossing the two $1.25 \times 25\,\mathrm{cm}^2$ wire pads in the centre of the beam, for two HV settings.

stand in detail the electrical properties of the design. The sizes of capacitances between readout pads and ground and mutual capacitances were simulated. This effects the efficiency and cross talk rate expected. They were compared to measurements of the chamber after the November testbeam. The measurements were in good agreement with the simulations although several construction faults were uncovered and repaired before the April testbeam.

The response of the chamber to minimum ionising particles was measured with data taken in two testbeam periods. The readout was based upon the ASDQ++ chip. The chamber demonstrated the required response needed for the muon detector. An unfortunate feature in the baseline restorer was observed in the ASDQ chip leading to unforeseen "late" (out-of-time) cross talk, this was partially corrected in the April testbeam data. The FE-boards showed some unwanted noise and cross talk between channels. Modifications before the April testbeam have improved these greatly. The stability of the modified FE-boards still needs improvement in a system with more than one FE-board attached to the chamber.

The efficiency for both a double gap and two double gaps as a function of the HV was measured. The efficiencies were over 95% for each double gap, for a sufficient range of HV to allow an increase in the HV if the gain begins to drop with aging of the chamber.

The cross talk in the cathode pads was small and fully under control, the cross talk between the wire pads was larger but still substantially less than the geometrical cross talk.

5 Acknowledgements

The authors would like to express their gratitude G. Chiodi and D. Marras for their help in constructing the electronics and to the PNPI group for their help in understanding the requirements for a successful chamber design. Also it is a pleasure to thank the CERN accelerator groups for the regular supply of pions to the two testbeam areas and the continuing support of CNPq for the project.

References

[1] B. Schmidt. LHCb muon system by numbers. LHCb Internal Note 2000-089, CERN, 2000.

[2] W. Riegler. Crosstalk, cathode structure and electrical parameters of the MWPCs for the LHCb muon system. LHCb Internal Note 2000-061, CERN, 2000.

[3] B. Bochin et al. Wire pad chamber for LHCb muon system. LHCb Internal Note 2000-003, CERN, 2000.

[4] W. Riegler. Detector physics and performance simulations of the MWPCs for the LHCb muon system. LHCb Internal Note 2000-060, CERN, 2000.

[5] W. Riegler B. Schmidt A. Kashchuk, L. de Paula and T. Schneider. Performace study of a MWPC prototype for the LHCb muon system with the ASDQ chip. LHCb Internal Note 2000-062, CERN, 2000.

[6] A. Kashchuk. Updated front end electronics system based upon the ASDQ chip (Prelimiary title). LHCb Internal Note 2001-0XX, CERN, 2001.